

Observation of Exotic Meson Production in the Reaction $\pi^- p \rightarrow \eta' \pi^- p$ at 18 GeV/c

E. I. Ivanov,¹ D. L. Stienike,¹ D. I. Ryabchikov,³ G. S. Adams,⁷ T. Adams,¹ Z. Bar-Yam,⁴ J. M. Bishop,¹ V. A. Bodyagin,⁵ D. S. Brown,⁶ N. M. Cason,¹ S. U. Chung,² J. P. Cummings,⁷ K. Danyo,² S. P. Denisov,³ V. A. Dorofeev,³ J. P. Dowd,⁴ P. Eugenio,⁴ X. L. Fan,⁶ R. W. Hackenburg,² M. Hayek,⁴ D. Joffe,⁶ I. A. Kachaev,³ W. Kern,⁴ E. King,⁴ O. L. Kodolova,⁵ V. L. Korotkikh,⁵ M. A. Kostin,⁵ J. Kuhn,⁷ V. V. Lipaev,³ J. M. LoSecco,¹ J. J. Manak,¹ J. Napolitano,⁷ M. Nozar,⁷ C. Olchanski,² A. I. Ostrovidov,⁵ T. K. Pedlar,⁶ A. V. Popov,³ L. I. Sarycheva,⁵ K. K. Seth,⁶ X. Shen,⁶ N. Shenhav,⁴ W. D. Shephard,¹ N. B. Sinev,⁵ J. A. Smith,⁷ S. A. Taegar,¹ A. Tomaradze,⁶ I. N. Vardanyan,⁵ D. P. Weygand,⁸ D. B. White,⁷ H. J. Willutzki,² M. Witkowski,⁷ and A. A. Yershov⁵
(E852 Collaboration)

¹University of Notre Dame, Notre Dame, Indiana 46556

²Brookhaven National Laboratory, Upton, Long Island, New York 11973

³Institute for High Energy Physics, Protvino, Russian Federation

⁴University of Massachusetts Dartmouth, North Dartmouth, Massachusetts 02747

⁵Moscow State University, Moscow, Russian Federation

⁶Northwestern University, Evanston, Illinois 60208

⁷Rensselaer Polytechnic Institute, Troy, New York 12180

⁸Thomas Jefferson National Accelerator Facility, Newport News, Virginia 23606

(Received 2 February 2001)

An amplitude analysis of an exclusive sample of 5765 events from the reaction $\pi^- p \rightarrow \eta' \pi^- p$ at 18 GeV/c is described. The $\eta' \pi^-$ production is dominated by natural parity exchange and by three partial waves: those with $J^PC = 1^{-+}, 2^{++},$ and 4^{++} . A mass-dependent analysis of the partial-wave amplitudes indicates the production of the $a_2(1320)$ meson as well as the $a_4(2040)$ meson, observed for the first time decaying to $\eta' \pi^-$. The dominant, exotic (non- $q\bar{q}$) 1^{-+} partial wave is shown to be resonant with a mass of $1.597 \pm 0.010_{-0.010}^{+0.045}$ GeV/c² and a width of $0.340 \pm 0.040 \pm 0.050$ GeV/c². This exotic state, the $\pi_1(1600)$, is produced with a t dependence which is different from that of the $a_2(1320)$ meson, indicating differences between the production mechanisms for the two states.

DOI: 10.1103/PhysRevLett.86.3977

PACS numbers: 13.85.Ni, 14.40.Cs, 25.40.Qa

Exotic mesons—those whose valence structure is not composed of a quark-antiquark ($q\bar{q}$) pair—have been discussed [1–10] for many years but have only recently been observed experimentally. The underlying structure of the observed exotic states at 1.4 GeV/c² decaying into $\eta \pi^-$ [11–13] and at 1.6 GeV/c² decaying into $\rho^0 \pi^-$ [14] is not yet understood. Possible explanations for these $I = 1$ states could be that they are hybrid mesons, consisting of a $q\bar{q}$ pair and a constituent gluon, or four-quark ($q\bar{q}q\bar{q}$) states. However, within the framework of the flux-tube model the masses of these states are somewhat low to be hybrid mesons [6]; and four-quark states are expected to be very broad [1].

Since the models for exotic mesons typically predict masses, widths, and branching ratios, and since it is important to classify the exotic states to provide necessary input to the QCD models, there is a strong motivation to search for additional states as well as to search for additional decay modes for the observed states. In this paper, we describe the search for exotic states decaying into the $\eta' \pi^-$ final state using the reaction $\pi^- p \rightarrow \eta' \pi^- p$, where $\eta' \rightarrow \eta \pi^+ \pi^-$ and $\eta \rightarrow \gamma \gamma$.

The data sample was collected during the 1995 run of experiment E852 at the Multi-Particle Spectrometer facility at Brookhaven National Laboratory (BNL). A π^- beam with laboratory momentum 18 GeV/c and a liquid hydro-

gen target were used. A detailed description of the experimental apparatus can be found elsewhere [12].

The trigger required three forward-going charged tracks, a charged recoil track, and a signal in a lead-glass electromagnetic calorimeter (LGD). A total of 165×10^6 triggers of this type were recorded. After reconstruction, 1.37×10^6 events satisfied the trigger topology and had two clusters in the LGD. The η signal is seen in the $\gamma \gamma$ effective mass distribution in Fig. 1(a). Applying kinematic

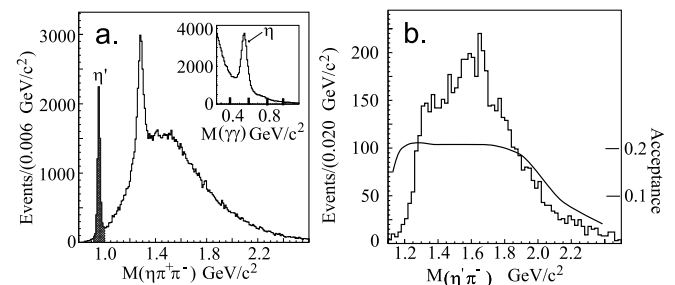


FIG. 1. (a) The $\eta \pi^+ \pi^-$ effective mass distribution for events consistent with the reaction $\pi^- p \rightarrow p \eta \pi^+ \pi^- \pi^-$ (two entries per event). The inset shows the $\gamma \gamma$ effective mass distribution in 0.01 GeV/c² bins. (b) The $\eta' \pi^-$ effective mass distribution. The distributions are uncorrected for acceptance. The smooth curve in (b) shows the true mass acceptance based upon the angular distributions determined in the partial-wave analysis.

fitting [15], some 70 000 events consistent with the $p\eta\pi^+\pi^-\pi^-$ ($\eta \rightarrow \gamma\gamma$) final state were found. These events satisfied energy-momentum conservation at the production and η decay vertices with a confidence level C.L. > 0.05 as well as the requirement that the difference between the azimuthal angles of the fitted proton direction and the measured proton track be less than 10° . As seen from the $\eta\pi^+\pi^-$ effective mass distribution (uncorrected for acceptance) in Fig. 1(a) the η' signal lies over an approximately 10% non- η' background. The second peak in the $\eta\pi^+\pi^-$ mass spectrum is due to production of the $f_1(1285)$ and $\eta(1295)$ resonances.

The next level of selection identified 6040 events consistent with the $p\eta'\pi^-$ ($\eta' \rightarrow \eta\pi^+\pi^-$, $\eta \rightarrow \gamma\gamma$) final state. These events satisfy energy-momentum conservation at the production, η' and η decay vertices with C.L. > 0.05 as well as topological and fiducial volume cuts. The resulting uncorrected $\eta'\pi^-$ mass spectrum [Fig. 1(b)] has a broad peak near $1.6 \text{ GeV}/c^2$ and structure around $1.3 \text{ GeV}/c^2$.

The acceptance-corrected distribution of the four-momentum transfer $|t|$ is shown in Fig. 2(a). The amplitude analysis discussed below was made for the data in the range $0.09 < |t| < 2.5 \text{ GeV}^2/c^2$. Because of the very low

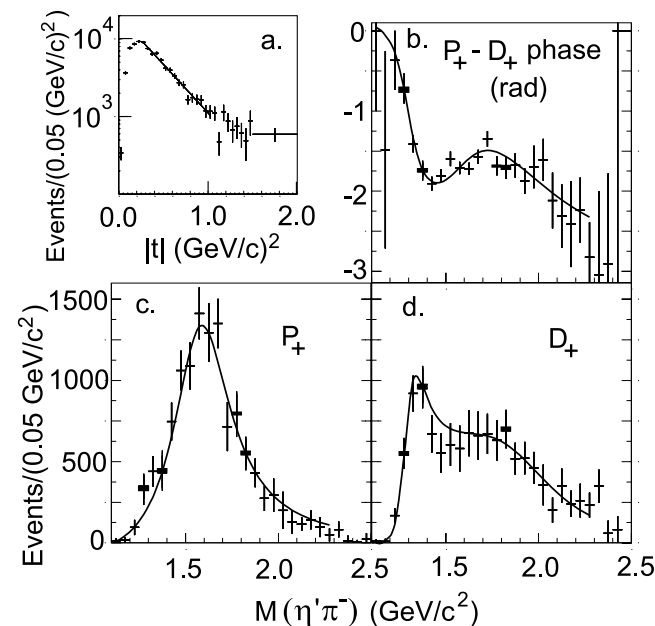


FIG. 2. (a) The acceptance-corrected $|t|$ distribution fitted with the function $f(t) = ae^{b|t|}$ (solid line). (b)–(d) The results of the mass-independent PWA (horizontal lines with error bars) and a typical mass-dependent fit (solid curve) using $0.05 \text{ GeV}/c^2$ mass bins. Only P_+ and D_+ partial waves and their phase difference are shown. The range of the ambiguous solutions is plotted with black rectangles. (b) The $(P_+ - D_+)$ phase difference. (c) The intensity distribution of the P_+ partial wave. (d) The intensity distribution of the D_+ partial wave. The solid curves in (b)–(d) show a mass-dependent fit (fit 1) to the P_+ and D_+ wave intensities and the $(P_+ - D_+)$ phase difference.

acceptance in the region $|t| < 0.09 \text{ GeV}^2/c^2$, the 275 events in that region were not used. In the interval $0.25 < |t| < 1.0 \text{ GeV}^2/c^2$ the $|t|$ distribution has an exponential behavior and can be fitted with the function $f(t) = ae^{b|t|}$ with $b = -2.93 \pm 0.11 (\text{GeV}/c)^{-2}$. The magnitude of b is significantly less than that observed for the $\eta\pi^-$ final state [11,12], where $b \approx -5 (\text{GeV}/c)^{-2}$ (see the discussion below).

A mass-independent partial-wave analysis (PWA) [12,16,17] of the data was used to study the spin-parity structure of the $\eta'\pi^-$ system. The partial waves are parametrized by a set of five numbers: $J^{PC}m^\epsilon$, where J is the angular momentum, P the parity, and C the C parity of the $\eta'\pi^-$ system; m is the absolute value of the angular momentum projection; and ϵ is the reflectivity (coinciding with the naturality of the exchanged particle [18]). We will use simplified notation in which each partial wave is denoted by a letter, indicating the $\eta'\pi^-$ system's angular momentum in standard spectroscopic notation, and a subscript, which can take the values 0, +, or −, for $m^\epsilon = 0^-, 1^+, \text{ or } 1^-$, respectively. We assume that the contribution from partial waves with $m > 1$ is small and can be neglected [12,19].

Mass-independent PWA fits shown in this paper are carried out in 0.05 and $0.10 \text{ GeV}/c^2$ mass bins from 1.1 to $2.5 \text{ GeV}/c^2$ and all use the $S_0, P_-, P_0, P_+, D_-, D_0, D_+$, and G_+ partial waves. For each partial wave the complex production amplitudes are determined from an extended maximum likelihood fit [17]. The spin-flip and spin-non-flip contributions to the baryon vertex lead to a production spin-density matrix with maximal rank two. A rank two mass-independent PWA in a system of two pseudoscalars cannot be performed because of the presence of a continuous mathematical ambiguity. Rank two fits were done when additional assumptions for the amplitudes were introduced (assumptions regarding the t dependence and mass dependence of the amplitudes) to resolve the continuous ambiguity problem, and they gave results consistent with those from the rank one fits. The PWA fits presented in this paper are with spin-density matrix of rank one.

The experimental acceptance was determined by comparison of the data with a Monte Carlo event sample. The Monte Carlo events were generated with isotropic angular distributions in the Gottfried-Jackson frame. The detector simulation was based on the E852 detector simulation package SAGEN [11,12]. The experimental acceptance was incorporated into the PWA by means of Monte Carlo normalization integrals [12]. The quality of the fits was determined by a χ^2 comparison of the experimental multipole moments with those predicted by the results of the PWA fit [19].

Results of the PWA are shown in Fig. 2 for the $0.05 \text{ GeV}/c^2$ fits and Fig. 3 for the $0.10 \text{ GeV}/c^2$ fits. The former are intended to show detail in the high statistics low-mass region and the latter are used to study the high-mass region. The unnatural-parity-exchange waves (not

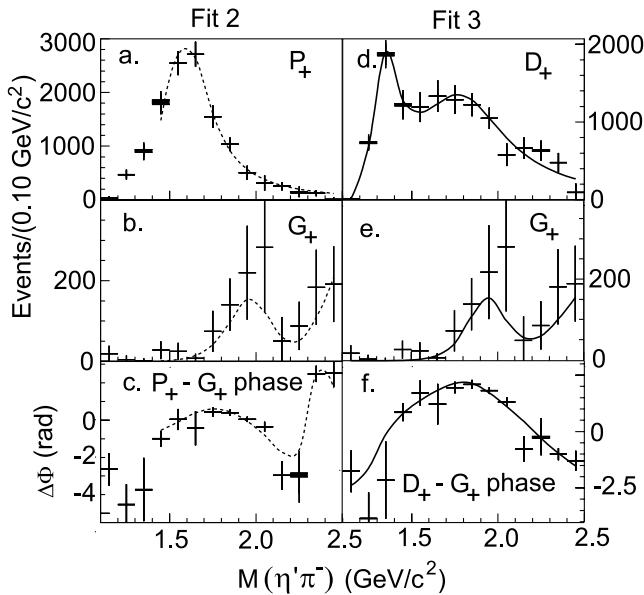


FIG. 3. The results of the mass-independent PWA (horizontal lines with error bars) and typical mass-dependent fits (solid and dashed curves) using $0.1 \text{ GeV}/c^2$ mass bins. (a)–(c) show the PWA and fit 2 (dashed curves) for the $P_+ - G_+$ intensities and their phase difference; (d)–(f) show the PWA and fit 3 (solid curves) for the $D_+ - G_+$ intensities and their phase difference. The range of the ambiguous solutions is plotted with black rectangles.

shown) are small, poorly determined, and do not affect our results.

The acceptance-corrected numbers of events predicted by the PWA fits for the stronger partial waves and the phase differences between them are shown as points with error bars. There are discrete mathematical ambiguities in the description of a system of two pseudoscalar mesons [17]. The ambiguous solutions were found by performing 1000 PWA fits with random starting values in each mass bin. The range of the ambiguous solutions in a mass bin is presented by black rectangles, and the maximum extent of their statistical errors is shown as the error bar. In most mass bins, the range of values found for the ambiguous solutions was small enough that they cannot be distinguished in the figures.

Between 1.5 and $1.8 \text{ GeV}/c^2$ the exotic P_+ is the dominant wave. Its intensity distribution consists of a broad structure peaked near $1.6 \text{ GeV}/c^2$. The D_+ wave intensity has a narrow peak at $1.3 \text{ GeV}/c^2$ associated with the $a_2(1320)$ and a broad structure at higher masses. The G_+ wave intensity is negligible below $1.7 \text{ GeV}/c^2$ and is clearly nonzero in the higher-mass region. The $(P_+ - D_+)$, $(D_+ - G_+)$, and $(P_+ - G_+)$ wave phase differences show rapid changes possibly indicative of the presence of interfering resonant states. The observed P_+ and D_+ intensities and their relative phase difference distribution are consistent with those reported by the VES [20] Collaboration. Leakage studies [12] were carried out and no leakage of significance was found among the dominant waves.

To study the nature of the observed partial waves, three different kinds of mass-dependent analyses (MDA) [12] have been carried out. In the first fit type (fit 1), the P_+ and D_+ intensities and their phase difference were fitted using the PWA results in $0.05 \text{ GeV}/c^2$ bins. For the other two types (fits 2 and 3), the P_+ and G_+ and the D_+ and G_+ waves, respectively, were fitted, along with their phase differences, using the $0.10 \text{ GeV}/c^2$ PWA results. These fits all used linear combinations of relativistic Breit-Wigner functions (poles) with mass-dependent widths and Blatt-Weisskopf barrier factors.

Because of the presence of distinct ambiguous PWA solutions in some mass bins, all possible combinations of these solutions were used as inputs to the MDA fits. Typical fits are shown as the smooth curves in Figs. 2 and 3. The fits use a single Breit-Wigner function to describe the P_+ wave, and two Breit-Wigner functions to describe both the D_+ and G_+ partial waves. [The fits can be improved by a second P_+ resonance in the $1.4 \text{ GeV}/c^2$ region corresponding to the $\pi(1400)$ state observed previously [11–13]. However, since the fits are satisfactory without the $\pi(1400)$, its production in this final state is not required in the analysis.]

Many acceptable mass-dependent fits ($\chi^2/\text{d.o.f.} < 1.5$) were obtained for each of the three fit types. The resonance parameters from these fits were all consistent with each other. Results from all of these fits were thus retained to determine resonance parameters. The resonance parameters are given in Table I for the P_+ exotic resonance and for the lower-mass resonances in the D_+ and G_+ waves. In this table, the central values for the mass and width of each resonance as well as the statistical error in these quantities were determined as the average of those quantities over all acceptable fits. The first error in these values is statistical, determined using the covariance matrix of the mass-independent PWA; the second is systematic. The systematic errors are based on the range of values allowed by taking into account different assumptions for the partial widths of the states, different parametrizations of the D_+ wave, and different ambiguous solutions. The experimental resolution has not been unfolded.

The mass and the width of the P_+ state are consistent with those of the $\pi_1(1600)$ exotic state observed in the $\pi^+\pi^-\pi^-$ system [14]. Our data are thus consistent with the observation of a second decay mode of the $\pi_1(1600)$.

The first pole in the D_+ partial wave has mass and width consistent with those of the $a_2(1320)$. The D_+ wave in the mass region above $1.4 \text{ GeV}/c^2$ is consistent with a broad Breit-Wigner function centered around $1.8\text{--}1.9 \text{ GeV}/c^2$

TABLE I. Fitted resonance parameters.

Partial wave	Mass	Width
P_+	$1.597 \pm 0.010^{+0.045}_{-0.010}$	$0.340 \pm 0.040 \pm 0.050$
D_+	$1.318 \pm 0.008^{+0.003}_{-0.005}$	$0.140 \pm 0.035 \pm 0.020$
G_+	$2.000 \pm 0.040^{+0.060}_{-0.020}$	$0.350 \pm 0.100^{+0.070}_{-0.050}$

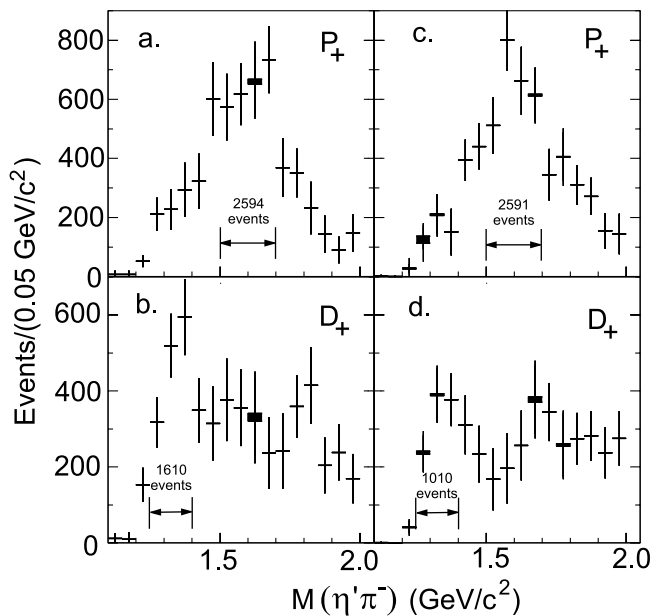


FIG. 4. (a),(b): Mass-independent PWA for $0.090 < |t| < 0.293 \text{ GeV}^2/c^2$; (c),(d): Mass-independent PWA for $0.293 < |t| < 2.5 \text{ GeV}^2/c^2$. The range of the ambiguous solutions is plotted with black rectangles.

and with width between 0.55 and $0.75 \text{ GeV}/c^2$. Alternatively, that mass region can be described with two narrower Breit-Wigner functions. The alternative parametrizations of the D_+ wave do not affect the conclusions of this paper.

The G_+ partial wave has been parametrized with two Breit-Wigner functions in fit types 2 and 3. The parameters of the lower-mass state given in Table I are consistent with the mass and width of the $a_4(2040)$ [21], which has not been observed previously in the $\eta'\pi^-$ system. The second Breit-Wigner pole in the G_+ wave is located in the high-mass region ($\approx 2.4 \text{ GeV}/c^2$) where limited statistics results in sizable statistical and systematic uncertainty. Its physical interpretation is unclear.

Mass-independent analyses have also been performed for two separate four-momentum-transfer intervals including equal numbers of events (see Fig. 4). The fits show that, as $|t|$ increases, the production rate for the $a_2(1320)$ decreases faster than the production rate for the exotic state. Note from Fig. 4 that the numbers of events in the marked peak bins for P_+ production are nearly equal for the two $|t|$ intervals (the ratio of the high- $|t|$ to the low- $|t|$ peaks is 1.00 ± 0.12) whereas for D_+ production, the ratio is 0.71 ± 0.15 . Since the $|t|$ distribution is correlated with the production mechanism for peripheral processes, we conclude that exotic meson production proceeds via a different production mechanism than that for production of

the $q\bar{q} a_2(1320)$ meson, or that it proceeds with a different mixture of the same production mechanisms.

In conclusion, we have studied the $\eta'\pi^-$ system produced in the reaction $\pi^- p \rightarrow p \eta'\pi^-$ at $18 \text{ GeV}/c$. We find that an exotic meson, the $\pi_1(1600)$ is produced, decaying to $\eta'\pi^-$. The different t dependence for their production shows that the well-known $a_2(1320)$ and the exotic $\pi_1(1600)$ are produced via different production mechanisms. Finally, a high-mass state consistent with the $a_4(2040)$ has been observed decaying to $\eta'\pi^-$.

We would like to express our appreciation to the members of the MPS group, and to the staffs of the AGS, BNL, and the collaborating institutions for their efforts. This research was supported in part by the National Science Foundation, the U.S. Department of Energy, and the Russian State Committee for Science and Technology. The Southeastern Universities Research Association (SURA) operates the Thomas Jefferson National Accelerator Facility for the United States Department of Energy under Contract No. DE-AC05-84ER40150.

- [1] R. L. Jaffe and K. Johnson, Phys. Lett. **60B**, 201 (1976); R. L. Jaffe, Phys. Rev. D **15**, 267 (1977).
- [2] T. Barnes and F. E. Close, Phys. Lett. **116B**, 365 (1982).
- [3] T. Barnes *et al.*, Nucl. Phys. **B224**, 241 (1983).
- [4] N. Isgur and J. Paton, Phys. Rev. D **31**, 2910 (1985).
- [5] I. Balitsky *et al.*, Z. Phys. C **33**, 265 (1986); J. I. Latorre, P. Pascual, and S. Narison, Z. Phys. C **34**, 347 (1987); J. Govaerts *et al.*, Nucl. Phys. **B284**, 674 (1987).
- [6] T. Barnes *et al.*, Phys. Rev. D **52**, 5242 (1995).
- [7] F. E. Close and P. R. Page, Nucl. Phys. **B443**, 233 (1995).
- [8] Y. Uehara *et al.*, Nucl. Phys. **A606**, 357 (1996).
- [9] P. Lacock, C. Michael, P. Boyle, and P. Rowland, Phys. Rev. D **54**, 6997 (1996); C. Bernard *et al.*, Nucl. Phys. B, Proc. Suppl. **53**, 228 (1997).
- [10] T. Barnes, Acta Phys. Pol. B **31**, 2545 (2000).
- [11] D. R. Thompson *et al.*, Phys. Rev. Lett. **79**, 1630 (1997).
- [12] S. U. Chung *et al.*, Phys. Rev. D **60**, 092001 (1999).
- [13] A. Abele *et al.*, Phys. Lett. B **423**, 175 (1998).
- [14] G. S. Adams *et al.*, Phys. Rev. Lett. **81**, 5760 (1998).
- [15] SQUAW kinematic fitting program, in O. I. Dahl *et al.*, University of California Report No. P-126, 1968 (unpublished).
- [16] J. P. Cummings and D. P. Weygand, Report No. BNL-64637, 1997 (unpublished).
- [17] S. U. Chung, Phys. Rev. D **56**, 7299 (1997).
- [18] S. Chung and T. Trueman, Phys. Rev. D **11**, 633 (1975).
- [19] E. Tatar, Ph.D. thesis, University of Notre Dame, Notre Dame, Indiana, 2000.
- [20] G. M. Beladidze *et al.*, Phys. Lett. B **313**, 276 (1993).
- [21] Particle Data Group, D. Groom *et al.*, Eur. Phys. J. C **3**, 15 (2000).